Analysis of a Position Sensorless Control of a Salient-Pole Synchronous Reluctance Machine from Standstill to High-Speed Range

Mario Nikowitz*, Matthias Hofer, Manfred Schrdl
Technische Universitt Wien
Gusshausstrasse 25/370-02
1040 Vienna, Austria
*Phone: +43 1 58801-370228
*Email: mario.nikowitz@tuwien.ac.at
URL: http://www.tuwien.ac.at

Keywords

≪Sensorless control≫, ≪Reluctance drive≫, ≪Synchronous motor≫, ≪AC machine≫, ≪Electrical drive≫.

Abstract

This paper discusses the position sensorless control of a salient-pole synchronous-reluctance machine (SynRM) whose performance is analysed. Depending on the rotational speed of the machine different methods have to be applied. At low-speed range the INFORM method is used, which is based on the magnetic anisotropy of the rotor. At high-speed range two different methods are implemented and compared. The first method is the Back-EMF model, which is based on the flux estimation by integrating the induced voltage. The second method, the short-circuit method, directly uses the measured electrical quantities to calculate the rotor position. No further integration or other dynamical operations are necessary, which increases the dynamic of the position sensorless control model. These mentioned position sensorless control methods were implemented and tested on a prototype to verify the performance of each algorithm.

Introduction

Synchronous Reluctance machines (SynRM) have become very popular for industry in the last years. This is caused by the simple, robust and low-cost setup of the used rotor design. Furthermore, the higher efficiency compared to the widely used induction motor (IM) is a major benefit of this motor type [1, 3, 4, 9]. Especially the SynRM in salient-pole configuration (see Fig. 1a), which is discussed in this paper, has an efficiency advantage over the flux-barrier rotor in the low-load range [7]. This advantage is caused by the current-independency of the rated quadrature inductance $l_{s,q}$ compared to the flux-barrier machine [8]. Combining this efficiency advantage with the replacement of the rotary encoder by mathematical equations leads to a competitive system for many drive applications.

Tab. I lists the key-data of the used prototype.

Maximum shaft power	185 W
Maximum shaft torque	0.6 N m
Nominal shaft speed	3000 rpm
Line current	1.5 A RMS
Line voltage	162 V RMS

Table I: Key data of the SynRM–prototype

Assigned jointly to the European Power Electronics and Drives Association & the Institute of Electrical and Electronics Engineers (IEEE)

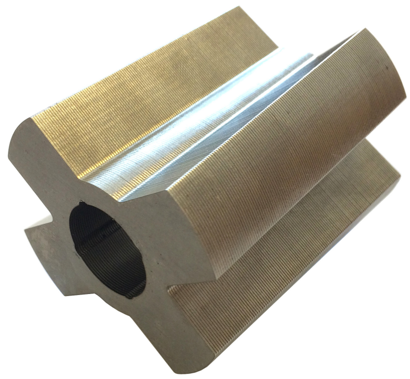

(a) SynRM rotor with salient poles.

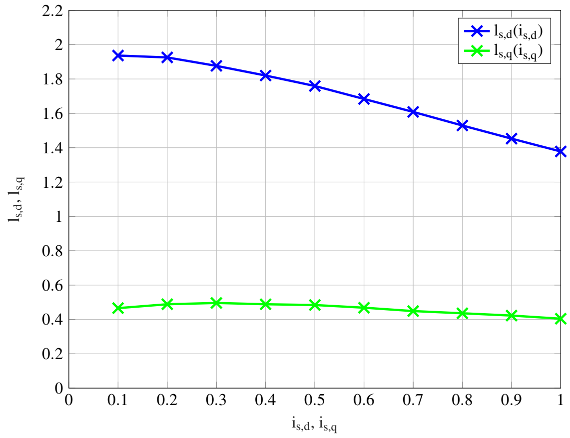

(b) Measured fundamental rated inductances as a function of rated current components $i_{s,d}$ and $i_{s,q}$.

Fig. 1: Salient pole SynRM–prototype.

Mathematical model of the SynRM

The common way to describe a SynRM is in the dq-reference frame. The direct axis (d-axis) is aligned in the direction of minimal magnetic reluctance, where the quadrature axis (q-axis) is aligned orthogonally to it. Because of the lack of permanent magnets the flux-linkage equation can be easily given by equation (1) and (2).

$$\psi_{s,d} = l_{s,d}(i_{s,d})\, i_{s,d} \tag{1}$$
$$\psi_{s,q} = l_{s,q}(i_{s,q})\, i_{s,q} \approx l_{s,q}\, i_{s,q} \tag{2}$$

The variables $l_{s,d}$ and $l_{s,q}$ represent the rated inductances of the motor, where their current dependency is shown in Fig. 1b. In the case of a salient pole SynRM the cross-coupling between the d- and the q-axis is negligibly small and can be ignored. With this machine specific equation the rated stator voltage can be described in the usual way as shown in eq. (3) and eq. (4).

$$u_{s,d} = r_s\, i_{s,d} + l_{s,d}(i_{s,d}) \frac{di_{s,d}}{d\tau} - \omega_m\, l_{s,q}\, i_{s,q} \tag{3}$$
$$u_{s,q} = r_s\, i_{s,q} + l_{s,q} \frac{di_{s,q}}{d\tau} + \omega_m\, l_{s,d}(i_{s,d})\, i_{s,d} \tag{4}$$

The rated stator resistance is represented by r_s, where ω_m symbolises the rated motor speed. Finally the rated torque of the SynRM is given by eq. (5).

$$t = -Im\left(\underline{\psi}_s\, \underline{i}_s^*\right) = \left(l_{s,d}(i_{s,d}) - l_{s,q}\right) i_{s,d}\, i_{s,q} \tag{5}$$

Position sensorless control methods

The choice of the position sensorless method mainly depends on the speed of the SynRM. For the low speed range the INFORM method is used [12]. This method is based on the rotor saliency, which is given by the difference of the inductances $l_{s,d}$ and $l_{s,q}$ (see Fig. 1b). At higher speeds the method must be changed to an EMF-based algorithm like the Back-EMF or the short-circuit method.

The INFORM method - Low speed range

The INFORM method is an anisotropy based position sensorless method [12]. It benefits from a large difference between the direct inductance $l_{s,d}$ and the quadrature inductance $l_{s,q}$, which is the also the main torque generation principle of the SynRM (see equation (5)). In the case of the salient pole SynRM a minimal difference of the inductances is always given (see Fig. 1b), what makes the INFORM method easier to handle compared to the flux barrier machine [10]. Basically, the rated inductances $l_{s,\alpha}$, $l_{s,\beta}$ and $l_{s,\alpha\beta}$ contain the information of the rotor position angle γ. In order to keep the calculation as simple as possible, the inverse inductance, the reluctance, is calculated. This reluctance is proportional to the current-slopes on which the INFORM calculation is based. Each PWM cycle the INFORM trajectory $\underline{c}_{INF}$ is calculated as shown in eq. (6).

$$\underline{c}_{INF} = \frac{\Delta i_U}{\Delta\tau} + \frac{\Delta i_V}{\Delta\tau} e^{j\left(\frac{4\pi}{3}\right)} + \frac{\Delta i_W}{\Delta\tau} e^{j\left(\frac{2\pi}{3}\right)} \tag{6}$$

A special PWM pattern generates the corresponding current-slopes to avoid interruptions of the current control caused by additional injected voltage pulses [6]. From the INFORM trajectory the rotor position angle γ can be calculated as described in eq. (7). Fig. 3a and Fig. 3c show the characteristic INFORM trajectories at no-load and at full load.

$$2\gamma_{INF} = \arg\left(\underline{c}_{INF}\right) \tag{7}$$

The INFORM method was tested on the prototype SynRM which was externally driven at constant speeds varying the torque to analyse the whole operating area. Fig. 2 shows the standard deviation σ of the position angle error $\Delta\gamma = \gamma_{INF} - \gamma_{Encoder}$ as a function of the rated torque t at different speeds ω_m. The probability density function (PDF) of the angle error is shown in Fig. 3b (no-load) and in Fig. 3d (full load).

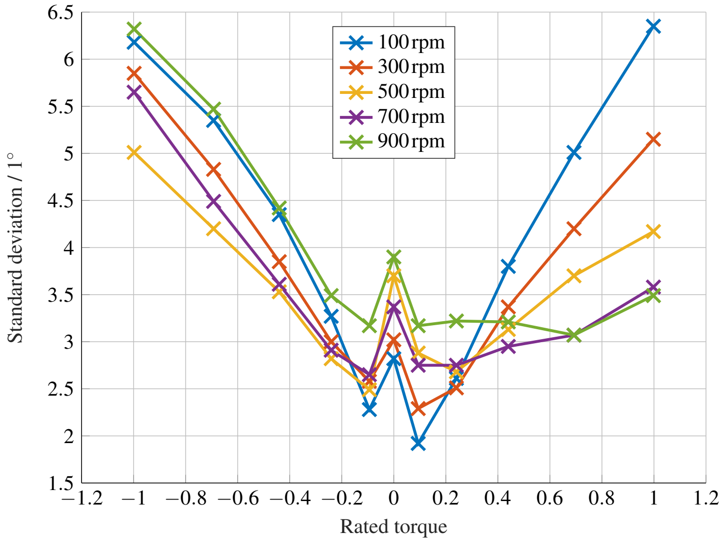

Fig. 2: Standard deviation σ of the INFORM angle error as a function of the rated torque for several speeds.

The INFORM method used on a SynRM motor has an inherent advantage caused by the same major principle, which is the necessary difference between the direct inductance $l_{s,d}$ and the quadrature inductance $l_{s,q}$. Especially in the case of a salient pole rotor there is no minimal saturation current in the

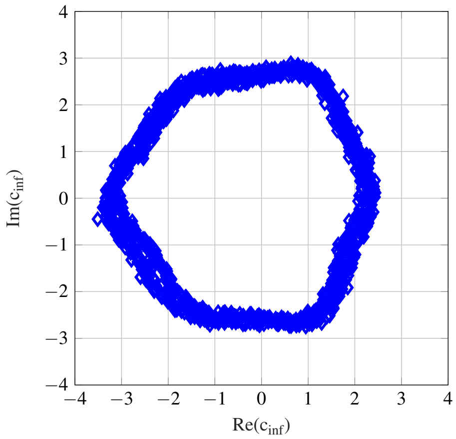

(a) INFORM trajectory $\underline{c}_{INF}$ at 100 rpm and at no-load.

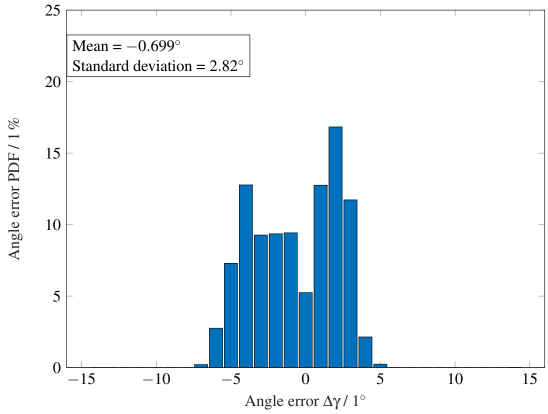

(b) Probability density function of the sensorless angle error $\Delta\gamma$ at 100 rpm and no-load ($\mu = -0.699°$, $\sigma = 2.82°$).

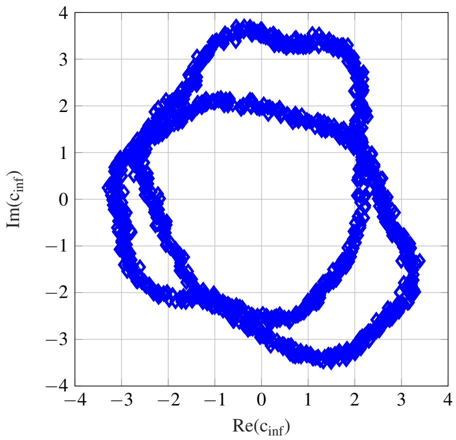

(c) INFORM trajectory $\underline{c}_{INF}$ at 100 rpm and at full-load.

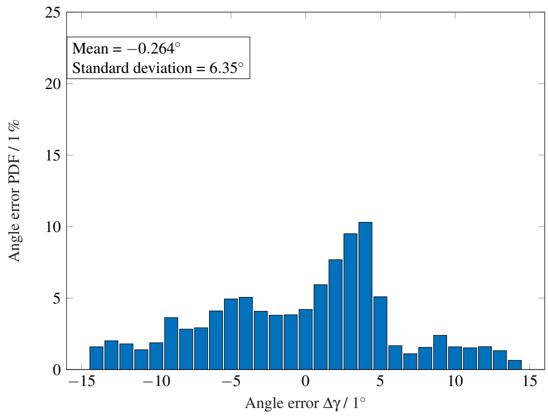

(d) Probability density function of the sensorless angle error $\Delta\gamma$ at 100 rpm and full-load ($\mu = -0.264°$, $\sigma = 6.35°$).

Fig. 3: Experiments regarding the INFORM method at 100 rpm.

q-axis necessary ($i_{s,q,min} = 0$) to get enough saliency compared to the flux barrier rotor [10]. With a maximum standard deviation of the angle error $\Delta\gamma$ less than 6.5° a sufficiently accurate sensorless method is achieved.

The Back-EMF method - high speed range

The Back-EMF method estimates the flux-linkage space-vector $\underline{\psi}_s$, which is rigidly connected to the rotor. For this purpose the induced voltage is integrated as shown in eq. (8).

$$\underline{\psi}_{s,\alpha\beta} = \int \left(\underline{u}_{s,\alpha\beta} - r_s\, \underline{i}_{s,\alpha\beta}\right) d\tau \tag{8}$$

The offset angle in the dq-reference frame, which results from the flux generation of the SynRM (see eq. (1) and eq. (2)), has to be subtracted to get the position of the d-axis of the rotor as shown in eq. (9) [5, 6].

$$\gamma_{BEMF} = \arg\left(\underline{\psi}_{s,\alpha\beta}\right) - \arg\left(\underline{\psi}_{s,dq}\right) \tag{9}$$

The major problem of this method is that there has to be a minimal flux-linkage in the motor to calculate the rotor position. This fact is a big problem in the case of SynRMs. Because of the lack of permanent magnets the flux-linkage has to be generated by the stator current. Fig. 4 shows the capability of the SynRM to produce flux-linkage. The reference flux-linkage $\psi_{s,ref}$ was calculated according to eq. (1) and eq. (2) and the non-linear inductances (see Fig. 1b), where the measured flux-linkage $\psi_{s,act}$ was determined by eq. (8).

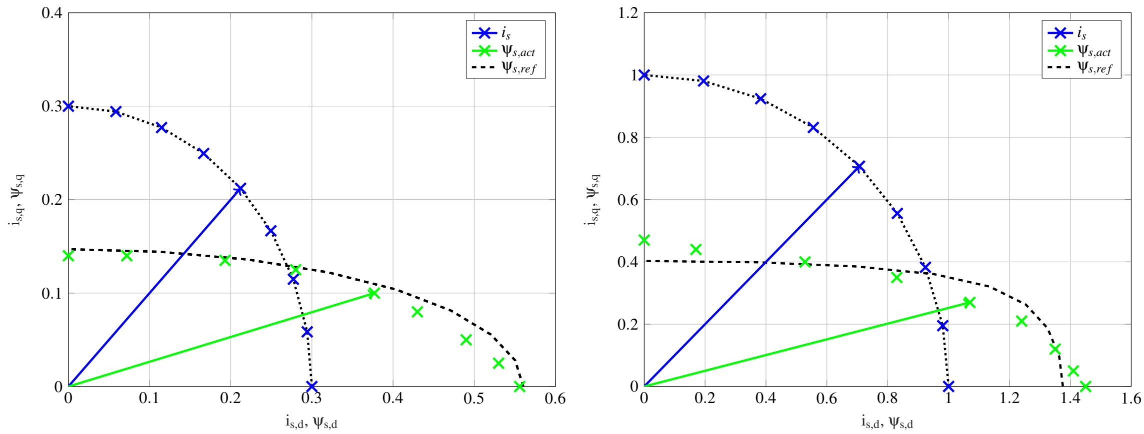

(a) Measured rated flux-linkage at 2000 rpm and low load, $|\underline{i}_s| = 0.3$.

(b) Measured rated flux-linkage at 2000 rpm and full-load, $|\underline{i}_s| = 1.0$.

Fig. 4: Capability of flux-linkage generation of the SynRM with salient poles.

Obviously a minimal direct current $i_{s,d,min,BEMF}$ is necessary to produce enough flux-linkage. The reason why a minimal d-current is needed is because of the larger inductance in the d-axis compared to the q-axis ($l_{s,d} > l_{s,q}$) (see Fig. 1b). Thus, a minimal direct current of $i_{s,d,min,BEMF} = 0.7$ was applied to operate the SynRM as a virtual permanent magnet synchronous motor (vPMSM) [2]. This operation mode increases the stability of the Back-EMF model significantly which however reduces the efficiency of the motor in the low load range [5, 6].

Experiments on the motor verify the functionality of this algorithm, where the motor was driven at constant speed and the SynRM was in a torque controlled operation mode. Fig. 5 shows the standard deviation of the position angle error $\Delta\gamma = \gamma_{BEMF} - \gamma_{Encoder}$ as a function of the rated torque t at different speeds ω_m.

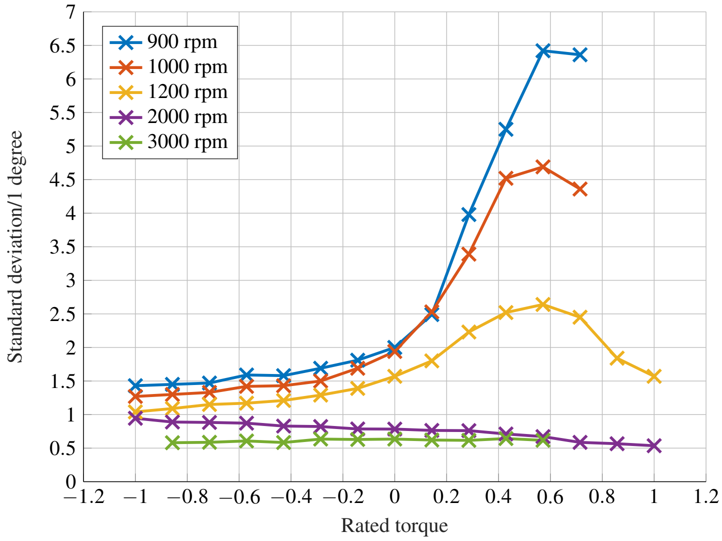

Fig. 5: Standard deviation σ of the Back-EMF angle error as a function of the rated torque for several speeds.

Because of the quite high minimal direct current $i_{s,d,min,BEMF} = 0.7$ there is a very low dependency on the load, caused by the nearly constant magnetic operation point of the SynRM. Fig. 6 demonstrates this fact by comparing the probability density function (PDF) of the position angle error $\Delta\gamma$ at no-load and at full load.

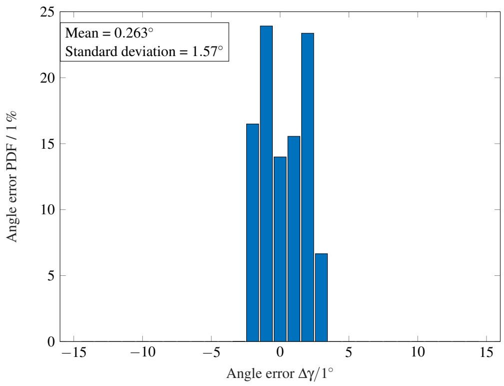

(a) Probability density function of the sensorless angle error $\Delta\gamma$ at 1200 rpm and at no-load ($\mu = 0.263°$, $\sigma = 1.57°$).

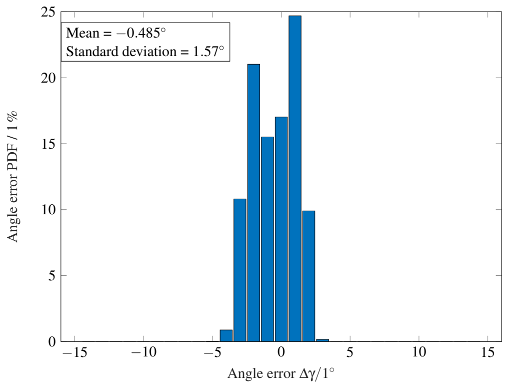

(b) Probability density function of the sensorless angle error $\Delta\gamma$ at 1200 rpm and at full load ($\mu = -0.485°$, $\sigma = 1.57°$).

Fig. 6: Experiments regarding the Back-EMF method at 1200 rpm.

The Short-Circuit method - high speed range

The Short-Circuit method is an EMF-based algorithm which does not need any information of the stator voltage of the SynRM [13]. This is achieved by using the short-circuits of the PWM pattern which clamp the stator voltage to $\underline{u}_s = 0$. The derivation of the Short-Circuit model starts with the transformation equation of the current-slope space vector $\frac{d}{d\tau}\underline{i}_s$ from the dq-reference frame to the $\alpha\beta$-reference frame, see eq. (10).

$$\frac{d}{d\tau}\underline{i}_{s,\alpha\beta} = \frac{d}{d\tau}\underline{i}_{s,dq} \cdot e^{j\gamma} \tag{10}$$

Assigned jointly to the European Power Electronics and Drives Association & the Institute of Electrical and Electronics Engineers (IEEE)

Calculating the argument of this equation and transforming it to the wanted rotor position angle γ results to eq. (11), which represents the basic equation of the Short-Circuit model.

$$\gamma = \arg\left(\frac{d}{d\tau}\underline{i}_{s,\alpha\beta}\right) - \arg\left(\frac{d}{d\tau}\underline{i}_{s,dq}\right) \tag{11}$$

So far the determination of the current-slope in the $\alpha\beta$-reference frame can easily be done by the current measurements. For the current-slope in the dq-reference frame we have to take a look at the stator voltage eq. (3) and eq. (4) (assuming $r_s \approx 0$) in the case of a short-circuit.

$$\underline{u}_{s,dq} = 0 = \frac{d}{d\tau}\underline{\psi}_{s,dq} + j\,\omega_m\,\underline{\psi}_{s,dq} \tag{12}$$

After transforming eq. (12) to $\frac{d}{d\tau}\underline{\psi}_{s,dq}$ and inserting the flux eq. (1) and eq. (2) we get eq. (13).

$$\begin{aligned}\frac{d}{d\tau}\left(l_{s,d}\,i_{s,d} + j\,l_{s,q}\,i_{s,q}\right) &= -\,j\,\omega_m\left(l_{s,d}\,i_{s,d} + j\,l_{s,q}\,i_{s,q}\right)\\ &= \omega_m\left(l_{s,q}\,i_{s,q} - j\,l_{s,d}\,i_{s,d}\right)\end{aligned} \tag{13}$$

Next the comparison of the coefficients leads to an expression for the current-slope in the dq-reference frame as shown in eq. (14).

$$\frac{d}{d\tau}\underline{i}_{s,dq} = \omega_m\left(\frac{l_{s,q}}{l_{s,d}}\,i_{s,q} - j\,\frac{l_{s,d}}{l_{s,q}}\,i_{s,d}\right) \tag{14}$$

Finally, inserting eq. (14) in eq. (11) leads to the wanted equation of the rotor position angle γ, see eq. (15).

$$\gamma_{SC} = \arg\left(\frac{d}{d\tau}\underline{i}_{s,\alpha\beta}\right) - \arg\left(\omega_m\right) + \arctan\left(\frac{l_{s,d}^2}{l_{s,q}^2}\,\frac{i_{s,d}}{i_{s,q}}\right) \tag{15}$$

To verify this theoretical approach the Short-Circuit model was implemented on the prototype drive system. The SynRM was externally driven at constant speed by the test bench motor, where the operating point was varied by the torque controlled SynRM. Fig. 7 shows the standard deviation σ of the position angle error $\Delta\gamma = \gamma_{SC} - \gamma_{Encoder}$ as a function of the rated torque t at different speeds ω_m.

Obviously the Short-Circuit model works better at higher loads, which is caused by the larger current-slopes $\frac{d}{d\tau}\underline{i}_s$. In the no-load case a minimal direct current $i_{s,d,min,SC} = 0.2$ is necessary to keep the method working. These current-slopes are essential for the Short-Circuit method (see eq. (15)), which are plotted in Fig. 8a and 8c. Fig. 8b and 8d show the corresponding probability density functions of the position angle error $\Delta\gamma$.

The major systematic benefit of this method is that no information of the stator voltage $\underline{u}_s$ is necessary, like needed in [11]. The measurement of the voltage would require additional voltage sensors, which increases the costs of the drive system, where the use of the target voltage of the current controller leads to uncertainties at lower voltage levels caused by the dead-time of the PWM module. Another big advantage, compared to the Back-EMF model, is that there is no need for an integration process in this method. Especially at low speed the integrator of the Back-EMF method has to deal with drift

Assigned jointly to the European Power Electronics and Drives Association & the Institute of Electrical and Electronics Engineers (IEEE)

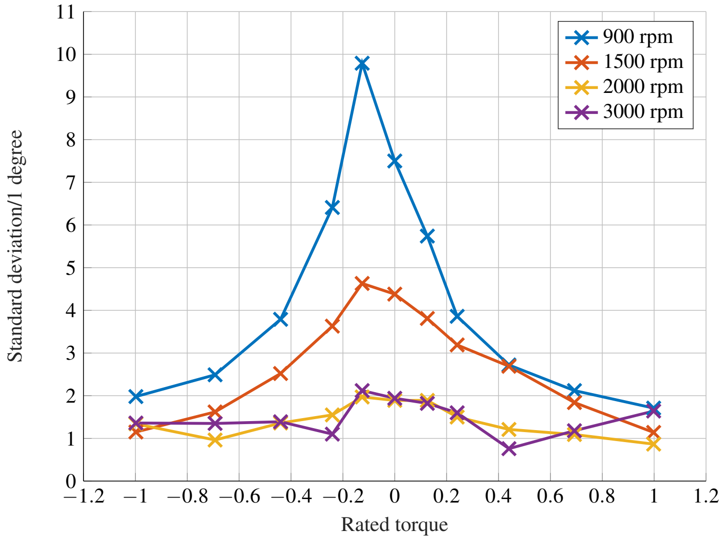

Fig. 7: Standard deviation σ of the Short-Circuit angle error as a function of the rated torque for several speeds.

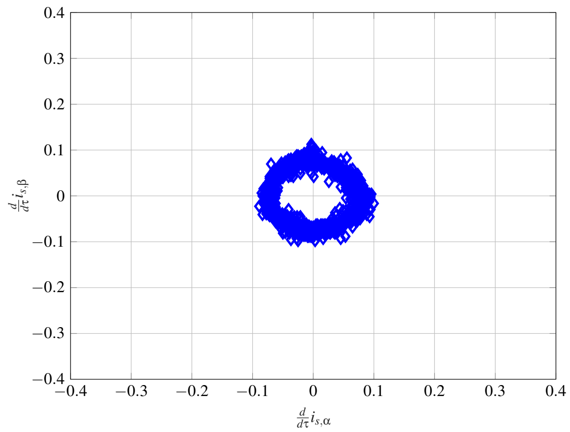

(a) Trajectory of the current-slope $\underline{i}_{s,\alpha\beta}$ at 1500 rpm and at no-load.

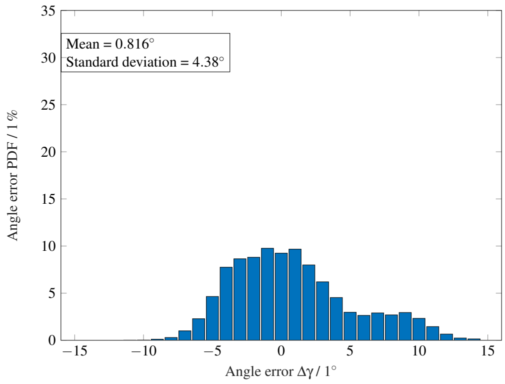

(b) Probability density function of the sensorless angle error $\Delta\gamma$ at 1500 rpm and at no-load ($\mu = 0.816°$, $\sigma = 4.38°$).

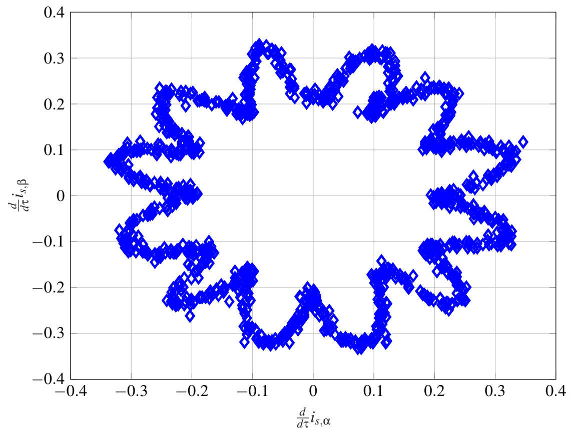

(c) Trajectory of the current-slope $\underline{i}_{s,\alpha\beta}$ at 1500 rpm and at full-load.

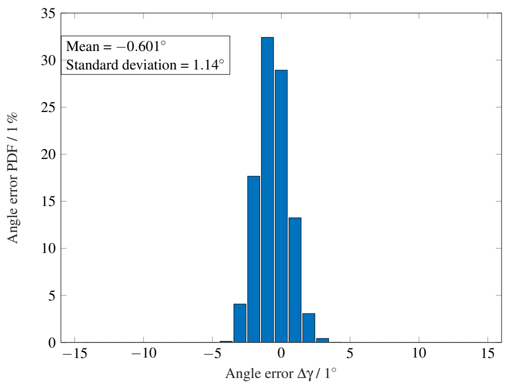

(d) Probability density function of the sensorless angle error $\Delta\gamma$ at 1500 rpm and at full-load ($\mu = -0.601°$, $\sigma = 1.14°$).

Fig. 8: Experiments regarding the Short-Circuit method at 1500 rpm.

phenomena, which reduces the stability of the dynamic system dramatically. Each time calculating the Short-Circuit method a current rotor position angle is estimated, which results in an independency of previous calculations of this sensorless method.

Position sensorless speed control

Finally, a speed controlled drive system was implemented, which covers the whole speed range from standstill up to 3000 rpm. Fig. 9a shows the test sequence of this operation mode which starts at standstill, accelerates up to 3000 rpm to brake down the machine to standstill again. Hence, the SynRM is successfully tested in a motor as well as in a generator operation mode.

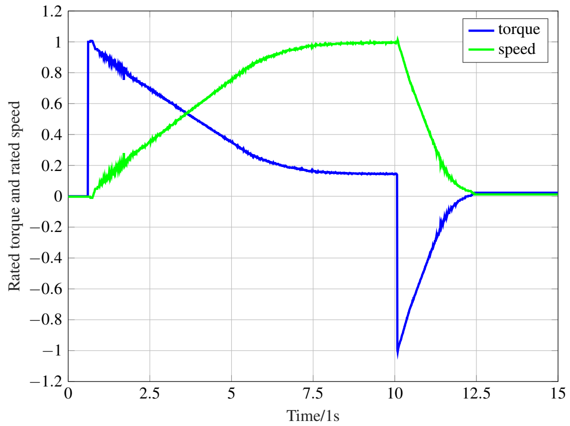

(a) Start up with high inertia moment up to 3000 rpm and back to standstill.

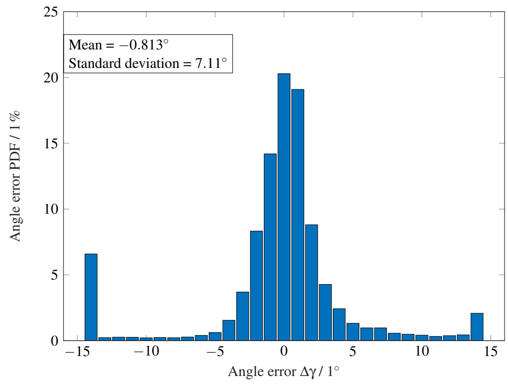

(b) Probability density function of the sensorless angle error $\Delta\gamma$ of the dynamic test ($\mu = -0.813°$, $\sigma = 7.11°$).

Fig. 9: Position sensorless speed control test sequence.

At low speed the INFORM method is used to estimate the rotor position angle γ. From a speed of $\omega_m = 0.25$ the angle error comes into an unacceptable range, thus a change of the sensorless method is recommended. Because of stability, accuracy and efficiency reasons the Short-Circuit model was chosen for the high speed area. The change of the model can also be seen in Fig. 9a, where the noise of the speed signal ω_m is abruptly reduced. Fig. 9b shows the probability density function of the rotor position error $\Delta\gamma$ over the whole test sequence. With a dynamic angle error standard deviation of $\sigma = 7.11°$ a sufficiently accurate sensorless operation for most applications can be achieved.

Conclusion

This paper presents three types of position sensorless methods to increase the economical benefit of the synchronous-reluctance machine in salient-pole configuration. At low-speed range, including standstill, the INFORM method is implemented. This position sensorless control uses the magnetic anisotropy of the rotor, which is the inherent function principle of a reluctance machine. At higher speeds the Short-Circuit model is the recommended sensorless method. Compared to the Back-EMF model the minimal $i_{s,d}$ is much smaller which increases the efficiency benefit of the drive system significantly. Also the robustness of the Short-Circuit model is better than the robustness of the Back-EMF model. Future works will focus on analysing the problems of the position sensorless operation of a SynRM using the Back-EMF model.

References

[1] A. Boglietti and M. Pastorelli. Induction and synchronous reluctance motors comparison. In *2008 34th Annual Conference of IEEE Industrial Electronics*, pages 2041–2044, Nov 2008.
[2] M. Bugsch, A. Held, and B. Piepenbreier. Sensorless control of synrms using an adaptive 2dof current control including a comparison of two alternating hf signal injection-based methods. In *IECON 2016 - 42nd Annual Conference of the IEEE Industrial Electronics Society*, pages 2910–2916, Oct 2016.

[3] E. S. Calvo and D. Potoradi. Synchronous reluctance motors with and without permanent magnets for high performance low cost electrical drives. In *2015 5th International Electric Drives Production Conference (EDPC)*, pages 1–7, Sept 2015.
[4] J. Guedelhoefer, D. Strbac, and R. Gottkehaskamp. Optimization of synchronous reluctance rotors as replacements for squirrel cages of small induction motors up to an iec frame of 90. In *IKMT 2015; 10. ETG/GMM-Symposium Innovative small Drives and Micro-Motor Systems*, pages 1–6, Sept 2015.
[5] M. Hofer, M. Nikowitz, and M. Schroedl. Application of a position sensorless control to a reluctance synchronous drive including flux weakening. In *PCIM Europe 2017; International Exhibition and Conference for Power Electronics, Intelligent Motion, Renewable Energy and Energy Management*, pages 1–7, May 2017.
[6] M. Hofer, M. Nikowitz, and M. Schroedl. Sensorless control of a reluctance synchronous machine in the whole speed range without voltage pulse injections. In *2017 IEEE 3rd International Future Energy Electronics Conference and ECCE Asia (IFEEC 2017 - ECCE Asia)*, pages 1194–1198, June 2017.
[7] M. Hofer, M. Nikowitz, and M. Schroedl. Power and efficiency of salient pole and flux barrier type synchronous reluctance machines in low power drives. In *2018 20th European Conference on Power Electronics and Applications (EPE'18 ECCE Europe)*, pages 1–6, Sept 2018.
[8] M. Hofer and M. Schroedl. Comparison of a flux barrier and a salient pole synchronous reluctance machine for high rotational speeds in electric traction applications. In *2017 20th International Conference on Electrical Machines and Systems (ICEMS)*, pages 1–6, Aug 2017.
[9] V. Kazakbaev, V. Prakht, V. Dmitrievskii, S. Sarapulov, and D. Askerov. Comparison of power consumption of synchronous reluctance and induction motor drives in a 0.75 kw pump unit. In *2017 International Siberian Conference on Control and Communications (SIBCON)*, pages 1–6, June 2017.
[10] M. Nikowitz, M. Hofer, and M. Schroedl. Improvements on a sensorless controlled synchronous reluctance machine down to standstill. In *PCIM Europe 2018; International Exhibition and Conference for Power Electronics, Intelligent Motion, Renewable Energy and Energy Management*, pages 1–7, June 2018.
[11] D. Paulus, J. Stumper, P. Landsmann, and R. Kennel. Robust encoderless speed control of a synchronous machine by direct evaluation of the back-emf angle without observer. In *2010 First Symposium on Sensorless Control for Electrical Drives*, pages 8–13, July 2010.
[12] M. Schroedl and P. Weinmeier. Sensorless control of reluctance machines at arbitrary operating conditions including standstill. *IEEE Transactions on Power Electronics*, 9(2):225–231, Mar 1994.
[13] M. Schroedl and R. S. Wieser. Emf-based rotor flux detection in induction motors using virtual short circuits. *IEEE Transactions on Industry Applications*, 34(1):142–147, Jan 1998.

Assigned jointly to the European Power Electronics and Drives Association & the Institute of Electrical and Electronics Engineers (IEEE)